

EERA DeepWind'2014, 11th Deep Sea Offshore Wind R&D Conference

Dynamic analysis of a floating vertical axis wind turbine under emergency shutdown using hydrodynamic brake

K. Wang^{1,2}, M.O.L. Hansen^{2,3} and T. Moan^{1,2}

¹ NOWITECH, Norwegian University of Science and Technology, 7491 Trondheim, Norway

² Centre for Ships and Ocean Structures, Norwegian University of Science and Technology, 7491 Trondheim, Norway

³ DTU Wind Energy, Department of Mechanical Engineering, Technical University of Denmark, Lyngby, Denmark

Abstract

Emergency shutdown is always a challenge for an operating vertical axis wind turbine. A 5-MW vertical axis wind turbine with a Darrieus rotor mounted on a semi-submersible support structure was examined in this study. Coupled non-linear aero-hydro-servo-elastic simulations of the floating vertical axis wind turbine were carried out for emergency shutdown cases over a range of environmental conditions based on correlated wind and wave data. When generator failure happens, a brake should be applied to stop the acceleration of the rotor to prevent the rotor from overspeeding and subsequent disaster. In addition to the traditional mechanical brake, a novel hydrodynamic brake was presented to apply to the shutdown case. The effects of the hydrodynamic brake on the platform motions and structural loads under normal operating conditions and during the emergency shutdown events were evaluated. The use of both the hydrodynamic brake and mechanical brake was also investigated. The application of the hydrodynamic brake is expected to be efficient for rotor shutdown and for reducing the platform motions and structural loads.

© 2014 Elsevier Ltd. This is an open access article under the CC BY-NC-ND license

(<http://creativecommons.org/licenses/by-nc-nd/3.0/>).

Selection and peer-review under responsibility of SINTEF Energi AS

Keywords: Emergency shutdown; Floating vertical axis wind turbine; Platform motion; Hydrodynamic brake

1. Introduction

As wind turbines continue to extend to deep waters, different platforms are used as the floating support structures, such as spar, semi-submersible and TLP. Most studies in this field have focused on the design, structural integrity, platform motion and installation of floating horizontal axis wind turbines (FHAWTs) to better understand the performance of different concepts and provide a basis for detailed structural design. However, different concepts for floating vertical axis wind turbines (FVAWTs) have also been presented, including the DeepWind [1-3], VertiWind [4] and Aerogenerator X concepts [5], to evaluate their economic potential and technical feasibility. A novel concept combining the DeepWind 5-MW rotor [6] and DeepCwind floater of the OC4 project [7] has also been proposed, and a coupled non-linear aero-hydro-servo-elastic model for analyzing this concept has been established and accordingly verified [8].

Many different challenges arise when FVAWTs operate under various wave and wind environmental conditions. Under normal operating conditions, the rotor can experience aerodynamic loads with continuous variation contributed by the azimuthal position and turbulent wind. Considerable forces acting on the rotor with fixed blades can be produced in stormy weather at increased rotational speed. The blades may also be deformed or broken, and the tower could collapse in more severe cases. Thus, determining how to initiate the emergency shutdown of a wind turbine is one of the most important concerns. The blade pitch mechanism is not applied in VAWTs with a Darrieus rotor, unlike in HAWTs, and the mechanical brake is installed in a standard manner. Experience has shown that aerobrakes also need to be installed to keep the rotational speed down in emergency situations when the generator torque is lost due to grid loss and the mechanical brake fails. The mechanical brake usually acts as a parking brake to stop the machine for maintenance purposes, therefore, aerodynamic braking is used to decelerate the rotor firstly and then the mechanical brake torque can be quite low. Although the mechanical brake is also used to bring the rotor to a standstill during high wind shutdowns for the majority of HAWTs, it is not easily applied for large scale VAWTs. Spoilers, an efficient and simple type of aerobrakes, are plates used to increase aerodynamic drag. However, the spoilers are integrated with blades, and their efficiency is determined by involving aerodynamic calculation of the blades together.

The current work presents a novel concept for a hydrodynamic brake that is installed at the end of the extended shaft of a vertical axis wind turbine through the centre column of the floater. The studied FVAWT has a 5-MW Darrieus rotor mounted on a semi-submersible support structure. The global motion and dynamic structural response of the FVAWT are calculated for the case in which the hydrodynamic brake is activated during emergency shutdown.

2. Methodology

2.1. Floating Wind Turbine Model

The FVAWT considered in this study is composed of a 5-MW Darrieus rotor, a semi-submersible and three catenary mooring lines. The rotor is located on a main column as shown in Fig. 1a. There are three offset columns with pontoons around the main column. Each catenary mooring is attached to an offset column to provide horizontal restoring stiffness. All of the columns are connected by braces to form an integrated body. Good stability and stiffness are ensured by a large waterplane area moment of inertia to limit the platform pitch angle under wave and wind conditions. Both of the mooring lines and the floating support structure were originally developed for the DeepCwind project and also used for supporting a 5-MW HAWT in Phase II of the Offshore Code Comparison Collaboration Continuation (OC4) project. DeepCwind is a U.S. - based project aimed at generating field-test data for use in validating floating offshore wind turbine modeling tools. The OC4 project is a continuation of the OC3 project, and Phase II of the OC4 project involved modeling a semisubmersible floating offshore wind system [7]. Among various numerical codes, the FAST semi-submersible floating wind turbine numerical model was also validated by comparing with DeepCwind test data [9]. The Darrieus rotor was originally developed for the DeepWind project (2010-2014), which is a part of the FP7 European project [10]. Compared to the FVAWT of the OC4 project, the FVAWT uses the 5-MW Darrieus rotor instead of the NREL 5-MW reference turbine. The slight difference between the two floating concepts indicates that the floater must be slightly modified to adapt for the VAWT rotor, which is heavier than the HAWT rotor. The specification of the present FVAWT are detailed in [8].

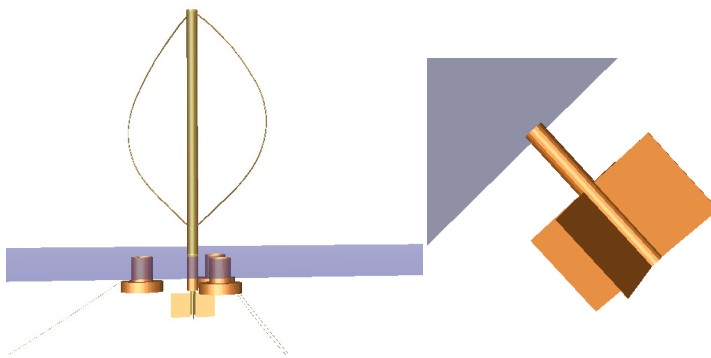


Fig. 1: (a) Floating vertical axis wind turbine; (b) Hydrodynamic brake

2.2. Coupled Time-Domain Analysis

The developed fully coupled simulation tool Simo-Riflex-DMS has the capability to carry out simulations of the dynamic motion of FVAWTs in the time domain. Thereby, the dynamic responses of a FVAWT can be calculated by integrating separate models of the wind inflow, aerodynamics, hydrodynamics, structural dynamics and controller dynamics. The tool couples three computer codes: Simo calculates the rigid body hydrodynamic forces and moments acting on the floater; Riflex models the blades, tower, shaft and mooring system as finite flexible elements, and provides the link to the DMS code and external controller; the DMS code calculates the forces on the blades based on an external aerodynamic module. The generator torque is written in Java. The Simo implementation computes the hydrodynamic loads at the actually displaced position of the floater, the DMS code calculates the aerodynamic loads on the blades and Riflex carries out full equilibrium iterations at each time step. This combination produces a comprehensive aero-hydro-servo-elastic simulation tool with sophisticated hydrodynamics, a stable non-linear finite element solver, well-known aerodynamics and a user-defined controller. The Simo-Riflex wind turbine module has been previously verified [11, 12], and the Simo-Riflex-DMS was presented and verified in [8].

In the aerodynamic load computation, the aerodynamic module is based on the Double Multiple Streamtube (DMS) model, which includes the effects of Reynolds number variations and incorporates the Beddoes-Leishman dynamic stall model. The turbulent wind field is generated by Turbsim. The code has been validated by comparison with existing experimental data [13]. The relative velocity sums up the incoming wind velocity at a certain point and the blade element velocity induced by platform motion and blade elastic deformation.

In the calculation of hydrodynamic loads carried out in this study, the floater was considered as a rigid body in Simo and the mooring line was represented as slender elements in Riflex. The hydrodynamic loads on the floater were handled by a linear potential flow model and the viscous term of the Morison formula, whereas the hydrodynamic loads on the mooring lines were represented using the Morison formula. The potential flow model produced added mass, radiation damping and first order wave forces in Wadam. The viscous forces were applied to represent the quadratic damping on the floater and mooring system. However, second order wave forces were not included in this model.

The structural dynamics of the rotor and mooring lines was calculated using the nonlinear finite element solver in Riflex. The rotor consisted of a tower and two blades, and their properties described in [10] were used to establish the structural model. Each blade, measuring 188.3 m in length, was modeled by 75 elements with two symmetry axes. The gyroscopic effects and the geometric stiffening effect were also considered.

A PI generator controller was employed in the control model. The objective of the control model was to enable variable speed operation maximizing power capture below the rated operation point and maintaining the generator speed above the rated operation point. The detailed controller strategy and relevant controller parameters are documented in [14], and their application in the integrated model used in this study has been verified in [8]. The notch filter used to reduce the effect of 2P variations was switched off in the present model.

2.3. Hydrodynamic Brake Model

Due to a lack of the blade pitch mechanism, the VAWT requires an additional device to stop the rotor under the emergency condition. In this study, a novel brake utilizing the drag force from water on the rotating plate was developed. The brake is composed of four plates and a centre column as shown in Fig. 2. The centre column of the brake provides enough buoyancy to balance the weight of the column itself and the four plates so that the brake does not affect the equilibrium condition of the floater. Under the normal operating conditions of the FVAWT, the centre column of the brake is connected to the floater. A device is assumed to enable the centre column to connect to the rotating shaft of the rotor during emergency shutdown. In this study, two hydrodynamic brakes were preliminarily designed. The dimensions of the centre column and the flat plate are detailed in Table 1.

In the hydrodynamic load calculation for the hydrodynamic brake, the hydrodynamic coefficients of the column and the plates are included in the model. Before the hydrodynamic brake is connected to the rotating shaft, it functions as a damping plate. The hydrodynamic loads on the brake can be calculated by the Morison formula. The brake can be divided into an upper part and a lower part. The upper part of the brake is the upper part of the centre column, which is a cylinder. Thus, the Morison formula for a cylinder is directly applied to the upper part. The added mass and drag coefficient for the upper part can be determined from the DNV standard [15]. The lower part is composed of the centre column and four flat

plates. The dimensional added mass in the Morison model is computed as indicated in Eq. 1 for horizontal forces acting on the combined column and flat plates and as indicated in Eq. 2 for vertical forces acting on the components. The drag force on the combined column and flat plates was considered to be equivalent to that on a thin plate, as in the DNV standard, thus, a drag coefficient of 1.9 was used in the model. The friction drag of flat plate parallel to the flow was neglected. The plate was modeled as a slender line on which the equivalent drag acted. Thus, the plate provided a damping effect in the translational degrees of freedom of the floater. After the centre column of the hydrodynamic brake is connected to the rotating shaft, it rotates along with the shaft to decelerate the rotor to a lower speed. The added mass and drag force in the translational degrees of freedom remains the same as that in the previous stage, whereas the drag in a rotational degree of freedom is newly generated. This drag force was represented as an additional torque acting on the column. The torque on this rotating flat plate was first computed from a simplified CFD model by using the sliding mesh technique. The relation between the estimated torque and the rotational speed was integrated into the model. In this manner, the effect of the hydrodynamic brake can be taken into account in the simulation. However, the damping effect in the yaw degree of freedom was neglected in the first stage because it is relatively small compared with that in the second stage. Furthermore, the interaction between the translational degrees of freedom and rotational degrees of freedom for the hydrodynamic brake was also neglected, thus, the complex model could be simplified and the main features maintained.

$$m_A^{hor} = \rho(1 - (r/b)^2 + (r/b)^4)\pi b^2 l_2 \tag{1}$$

$$m_A^{ver} = \rho C_A^{ver} \pi r^2 l_2 \tag{2}$$

Table 1: Hydrodynamic brake model

	Hydrobrake I		Hydrobrake II	
	Column	Plate	Column	Plate
Radius/Width (m)	1.5	11	2	16
Length (m)	38.494	36	30.494	28
Thickness (m)	0.02	0.083 ^a	0.02	0.083 ^b
Weight (N)	551509.2	3506517.8	583500.1	4765248.1
Bouyancy (N)	2736013.9	1321983.8	3853160.8	1495577.7

^a Sum of the hollow thickness and plate thickness of 0.014 m

^b Sum of the hollow thickness and plate thickness of 0.017 m

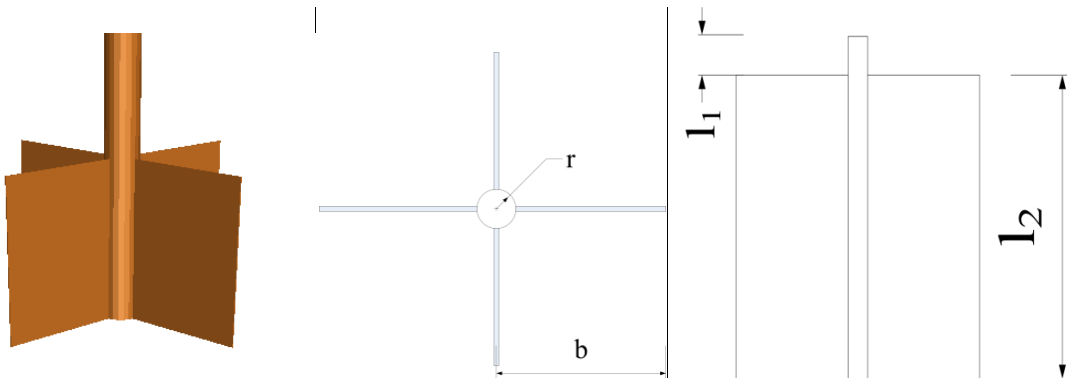


Fig. 2: Hydrodynamic brake

2.4. Environmental and Shutdown Conditions

A set of environmental conditions were prescribed for the FVAWT in the simulations. Six conditions with correlated and directionally aligned wind and waves were applied as listed in Table 2. For the wind conditions, both the normal wind profile model (NWP) and the normal turbulence model (NTM) were used in all of the cases. For the NWP conditions, the wind profile $U(z)$ is the average wind speed, as a function of height z above the free water level, given by the power law

$$U(z) = U_{\text{ref}} \left(\frac{z}{z_{\text{ref}}} \right)^{\alpha} \quad (3)$$

where U_{ref} is the reference wind speed, z_{ref} is the height of the reference wind speed and α is the power law exponent. For this study the value of z_{ref} was set to 79.78 m (vertical center of blades) above mean sea level and the value of α was set to 0.14 for the floating turbine according to IEC 61400-3 [16]. For the NTM conditions, three-dimensional turbulent wind fields were generated using NREL's TurbSim program [5] based on the Kaimal turbulence model for IEC Class C. For the wave conditions, the significant wave height (H_s) and peak period (T_s) were set based on the correlation with wind speed for the Statfjord site in the North Sea [17]. Then, wave time series were generated from JONSWAP spectra in the Simo program [18].

Table 2: Combined wind and wave conditions

	Uw (m/s)	Hs (m)	Tp (s)	Turb. Model	Fault Configuration	Sim. Length
LC 1	8	2.55	9.86	NTM	A, B, C, D	2800
LC 2	10	2.88	9.98	NTM	A, B, C, D	2800
LC 3	14	3.62	10.29	NTM	A, B, C, D	2800
LC 4	18	4.44	10.66	NTM	A, B, C, D	2800
LC 5	22	5.32	11.06	NTM	A, B, C, D	2800
LC 6	25	6.02	11.38	NTM	A, B, C, D	2800

- A) The original FVAWT without hydrodynamic brake and no fault occurrence
- B) The FVAWT with hydrodynamic brake I and no fault occurrence
- C) The FVAWT with hydrodynamic brake I and fault occurrence, followed by free rotation
- D) The FVAWT with hydrodynamic brake II and fault occurrence, followed by shutdown

Emergency shutdown is required to prevent the rotor from overspeeding after grid loss occurs. Accidental grid loss was assumed to occur at time $TF = 1200$ s, and the hydrodynamic brake was connected to the rotating shaft to initiate the shutdown process with a short time delay $TD = 1$ s. It should be noted that the TD was assumed based on the use of 0.1-s time delay between the moment of fault occurrence and the initiation of shutdown for a floating horizontal wind turbine [19]. To ensure the reaction process is conservative, a value 10 times the 0.1-s time delay was used in the simulation.

3. Torque estimation of the hydrodynamic brake

3.1. CFD Model of Hydrodynamic Brake

The concept of the hydrodynamic brake originated from the process of stir mixing of different liquids [20-23] and the high shear powder mixers used in the chemical industry [24, 25]. In addition to the flow features, turbulent kinetic energy and particle motion, the agitation torque is also calculated by numerical simulation and investigated by experiment. Although a wide variety of agitators are used for different mixing and agitation applications and although the researchers have postulated that an impeller with more baffles exhibit better performance in terms of power consumption, the simplest flat plates were proposed as a hydrodynamic brake in this work. Computational fluid dynamics (CFD) has already been used in many studies to predict the dynamics of the stir process. Therefore, the commercial CFD software FLUENT was used to simulate the hydrodynamic brake proposed in this study.

Two commonly used models the capability of computing the flow field for the rotating flow problem are the multiple reference frame (MRF) and the sliding mesh approach. When applying these models, the computational domain is divided into an inner region containing the rotating plate and an outer region of stationary flow. For the MRF model, the steady state computation, producing a time average flow field, is conducted with a rotating reference frame in the inner region and a stationary reference in the outer region, whereas the sliding mesh approach, based on transient computation to produce a time accurate flow field, allows the inner region to slide relative to the outer region in discrete time steps and carries out time-dependent computations using implicit or explicit interpolation of data at successive time steps. Therefore, the sliding mesh approach, as the more accurate model for simulating the flow rotation problem, was used in the simulation.

Because the length of the brake is long, a 2D model was established so as to reduce the computational cost and simplify the CFD model. The difference between the hydrodynamic brake model and the agitation model in the stirred tank is the definition of the boundary conditions according to the physical background. The infinite region in this model replaces a defined tank, so a sufficiently large outer region was built to eliminate the wall effect. The resolution of the computational grid is a key factor in any CFD simulation because it is related to the simulation accuracy and computational cost. Based on a preliminary convergence study, a grid mesh with 135900 cells for the inner region and 24640 cells for the outer region was established, as shown in Fig. 3a. For the discretization scheme, the first-order upwind was used because the choice of the discretization scheme has no effect on the mean velocities, as concluded by Aubin [23]. Furthermore, the absolute velocity formulation and Renormalized Group (RNG) $k-\epsilon$ turbulence model with a standard wall function for near-wall treatment were used in the simulation because the effect of swirl on turbulence is included in the RNG model, enhancing the accuracy for swirling flows. The size of the time step plays a significant role on the simulation accuracy in this model, and thus, the results could vary largely. Therefore, the time step was set to 0.1 s, providing an acceptable level of accuracy and an acceptable computational cost.

3.2. Estimation of Torque

The hydrodynamic character of the hydrodynamic brake was investigated and detailed information regarding the flow field, such as the pressure and velocity of the rotational flow, could be obtained. Fig. 3b shows an example of the velocity distribution around the brake. One of the most important hydrodynamic parameters is the relationship between the torque on the brake from water and the rotational speed of the brake, by understanding this relationship, the relevant coefficients can be implemented in the coupled model. After a series of simulations were performed with different rotational speeds, the agitation torques corresponding to each rotational speed could be determined. By multiplying the length of the plate, the relationship between the total torque and the rotational speed of hydrodynamic brake I was plotted, as shown in Fig. 4. A three order polynomial with unit of kNm was used to fit the relationship:

$$T_q = -20229\omega^3 + 125338\omega^2 - 30925\omega + 2680.2 \quad (4)$$

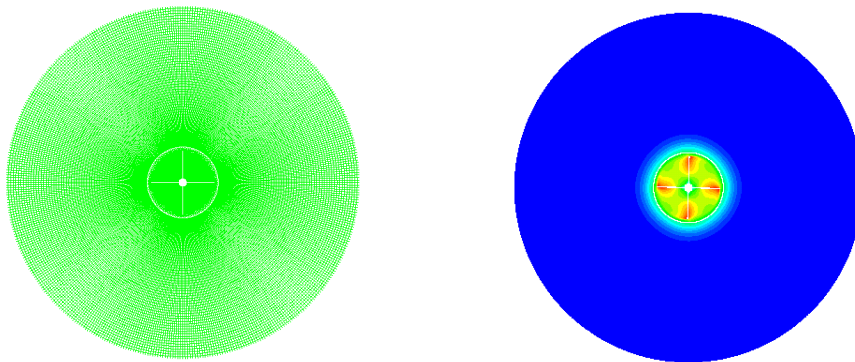


Fig. 3: (a) 2D mesh of hydrodynamic brake; (b) An example of velocity distribution at a rotational speed of 0.5 rad/s

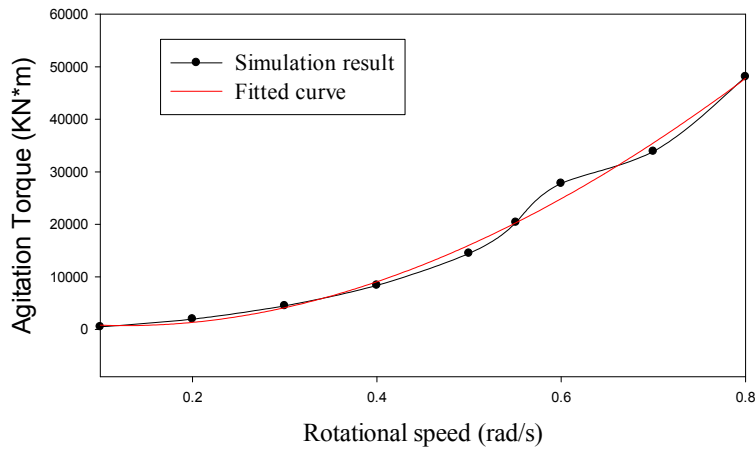


Fig 4: Relationship between rotational speed and torque

A similar method was used to determine the relationship between the torque and rotational speed for hydrodynamic brake II:

$$T_q = 123523\omega^3 + 21286\omega^2 + 9917.4\omega + 19.624 \quad (5)$$

4. Results

4.1. Effect of Hydrodynamic Brake I

The addition of the hydrodynamic brake to the original FVAWT concept may change the properties of the platform and subsequently the dynamic responses of the global motion and structural responses of the wind turbine. To evaluate the effect of the hydrodynamic brake, numerical simulations of the FVAWT with brake I and the original FVAWT without any brake installed were carried out to obtain the responses of the global motion of the platform, bending moment of the tower base and the mooring line tension. Then, the responses of these two structures were investigated.

The results of the comparison are summarized as follows:

- 1) In the load case with lower wind speed, the hydrodynamic brake has a less effect on the surge motion, as shown in Fig. 5. When the wind speed increases, the platform with the brake has much less response at the surge resonance frequency than the platform without the brake. The response near the wave frequency slightly decreases. The drag force from water on the brake actually introduces rather strong damping effect on the platform, and the damping increases with the relative velocity between the platform and wave velocity. A similar effect on the sway motion can be observed, but the difference is that the brake introduces a slightly stronger wave frequency response in sway motion. The brake hardly affects the heave motion of the platform because the drag force on the column associated with the heave motion is relatively small and the natural frequency of the heave motion lies outside the range of wave and wind frequencies.
- 2) Fig. 6 compares the power spectra of the roll motion between the platform with the brake and the original platform under load cases 1 and 3. The brake can decrease the natural period of the roll motion of the platform and induce a larger peak at the roll resonance frequency when compared with the roll motion of the FVAWT without brake. On the other hand, the drag force on the brake can reduce the roll motion induced by the 2P frequency of approximately 1.1 rad/s. The 2P frequency originates from the characteristics of vertical axis wind turbines with two blades. Because the axis of rotation is not parallel to the wind direction and the angle of attack of the blades varies with the azimuthal position during operation, the aerodynamic loads vary within one revolution. For a two-blade wind turbine, the variation of the torque occurs twice per revolution and the 2P

variations lead to the 2P frequency. Not only are the generator torque and gird affected significantly but the structures are also subject to severer fatigue problems. However, the roll motion itself is relatively small under aligned wind and wave conditions, and the effect is not as significant. A similar effect can be observed for the pitch motion, as shown in Fig. 7. As the wind increases, the effect becomes increasingly apparent.

- 3) The brake can significantly reduce the mooring tension response to the wind excitation as shown in Fig. 8, whereas it induces larger peaks at higher frequencies. In addition to the peak at the 2P frequency, another peak at a higher frequency is observed, which should be induced by the eigenfrequency of the blade. With the increase in wind speed, the peak induced by the structural eigenfrequency becomes increasingly apparent.
- 4) The effect of the brake on the bending moment of the tower base in the fore-aft (FA) and side-side (SS) directions was also investigated, and the main difference is the larger peak at the 2P frequency for the FVAWT with the brake. The reason for this finding could be that the brake makes the platform much stiffer, and thus, the bending moment induced by the 2P frequency increases.

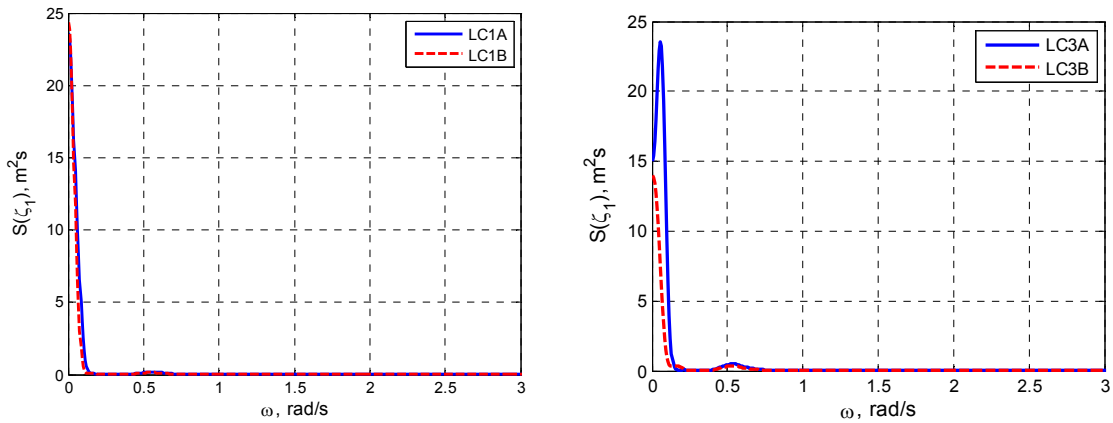


Fig. 5: Power spectra for surge motion of the platform for load cases 1 and 3 with fault configurations A and B

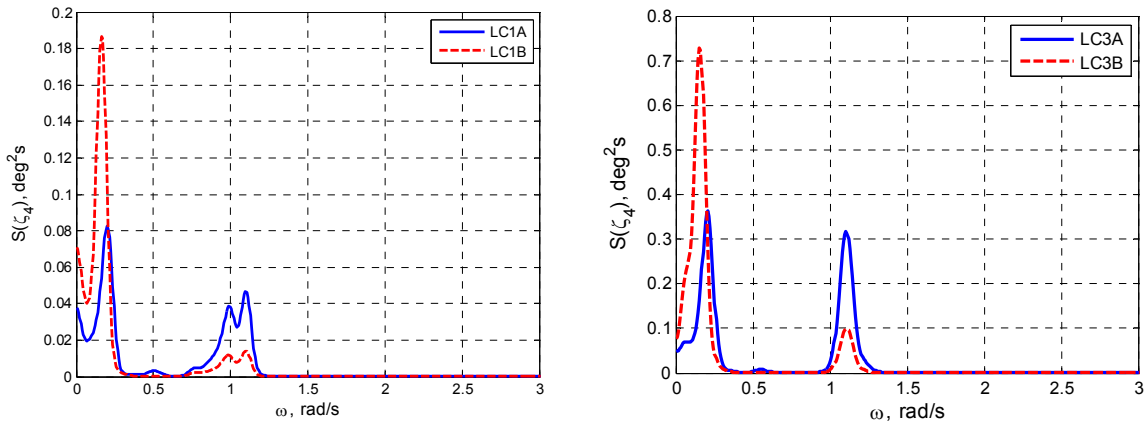


Fig. 6: Power spectra for roll motion of the platform for load cases 1 and 3 with fault configurations A and B

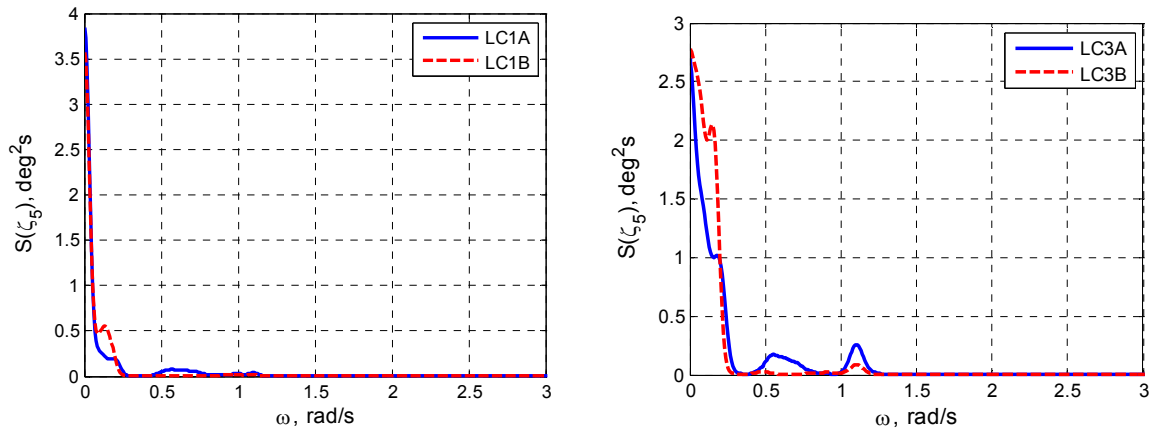


Fig. 7: Power spectra for pitch motion of the platform for load cases 1 and 3 with fault configurations A and B

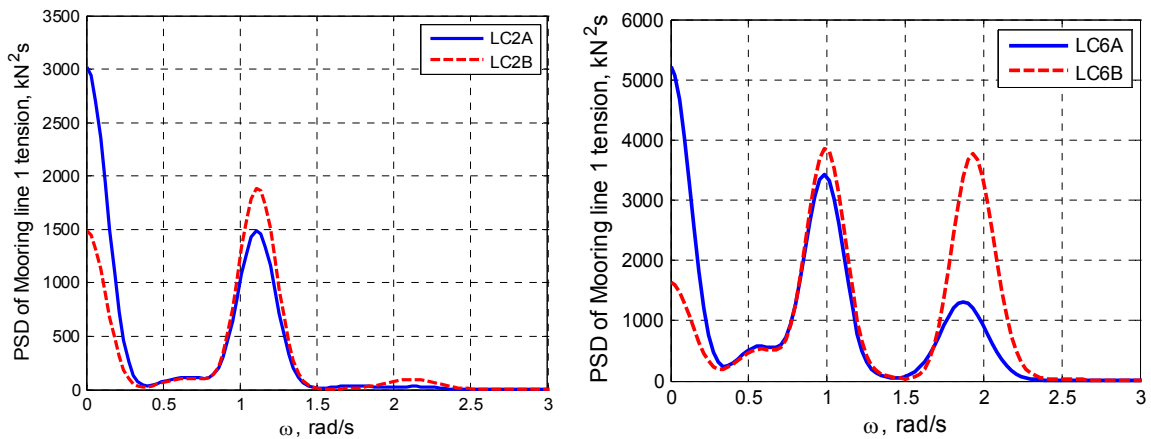


Fig. 8: Power spectra for mooring line tension for load cases 2 and 6 with fault configurations A and B

4.2. Analysis of Emergency Shutdown by Using Hydrodynamic Brake I

A fault, such as grid loss, was assumed to occur at 1200 s, at which point the wind turbine entered a state of free rotation without any generator torque or other torque to balance the aerodynamic torque before the brake connected to the rotating shaft of the wind turbine. Due to the large inertia of the wind turbine and variation of the aerodynamic torque, the increase in the rotational speed of shaft was not distinct. Once the hydrodynamic brake takes effect to counter the aerodynamic torque, the rotational speed varies depending on the difference between the aerodynamic torque and hydrodynamic torque on the brake. Fig. 9 shows a time series of the rotational speed of the rotor for different wind speeds. Brake I does not create enough torque to stop the rotation, but it can prevent the overspeeding of the rotor. Furthermore, the rotational speed decreases to a lower value for most wind speeds. If a mechanical brake is also applied at the same time, the shutdown of the wind turbine can be expected. However, the effect of the mechanical brake was not considered in this section. A further investigation was carried out for the global motion of the platform, mooring line tension and tower base bending moment when the brake was also rotating with the rotor.

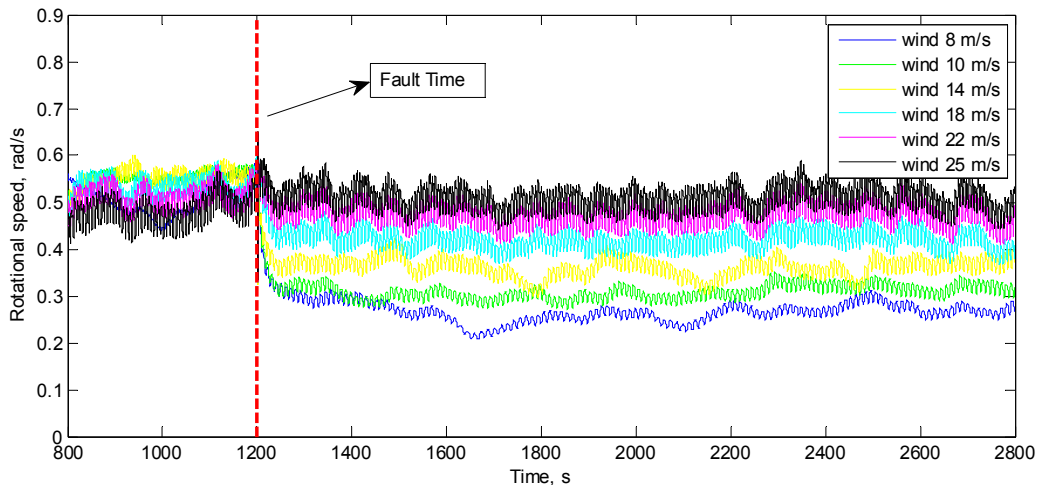


Fig. 9: Rotational speed for different wind speed after fault occurs at TF=1200 s by using brake I

Due to the decrease in the rotational speed after the activation of the hydrodynamic brake, the global motion of the platform shows better performance. Fig. 10 compares the global motion between fault configuration B and fault configuration C for different wind speeds. It can be observed that the surge and pitch motions are greatly enhanced, whereas the sway and roll motions experience both positive and negative effects under different load cases. However, the sway and roll motions are relatively small compared with the surge, pitch and yaw motions. Thus, the effect of the hydrodynamic brake on the sway and roll motions can be neglected. When the pitch motion was investigated using the power spectra shown in Fig. 11, it could also be observed that the decrease in the pitch motion mainly depended on the wind speed. The lower the wind speed was, the more the pitch motion was reduced. The peak at the 2P frequency still appeared, but the 2P frequency was reduced to a lower value corresponding to a lower rotational speed. A similar result was also observed for the roll motion, which decreased at the natural roll frequency and with a shift of 2P frequency. Furthermore, the peak of the roll response at higher structural frequency observed in the high wind case could be eliminated.

The mean tension of the three mooring lines was not significantly affected during the shutdown process by the hydrodynamic brake. The mean tension of mooring line 2 connected to the left column of the platform decreased slightly due to the decrease in the mean surge, whereas the mean tension of mooring line 3 connected to the right column of the platform increased slightly toward the mean tension of the mooring line 1 because of the decreased yaw motion. The standard deviations of the mooring lines were significantly reduced in most cases because the responses to the excitations due to the 2P frequency and the higher structural eigenfrequency were strongly weakened. The exceptions are the cases examined under high wind speeds. The 2P effect was reduced as the peak corresponding to the blade mode at its eigenfrequency was magnified at a wind speed of 22 m/s; On the other hand, the 2P effect was magnified as the peak at the structural eigenfrequency was reduced at a wind speed of 25 m/s. Therefore, the mooring line tension is sensitive to the rotational speed, which should be well configured to avoid exciting a 2P effect on the mooring line and inducing the structural eigenmodes.

Regarding the structural response, the bending moment of the tower base, which is one of the most important concerns under fault conditions, was also investigated. Both the mean values and standard deviations of the FA and SS tower base bending moments were significantly reduced, with the exception of the mean value of the FA tower base bending moment, at a high wind speed of 25 m/s. Because the rotational speed in load case 6C was not reduced, the thrust force due to the wind could still produce a large FA tower base bending moment. The activation of the brake together with the rotating shaft of the wind turbine could eliminate the 2P effect, thus allowing the wave frequency excitation to dominate the response of the FA tower base bending moment, as shown in the comparison between load cases 3B and 3C in Fig.12.

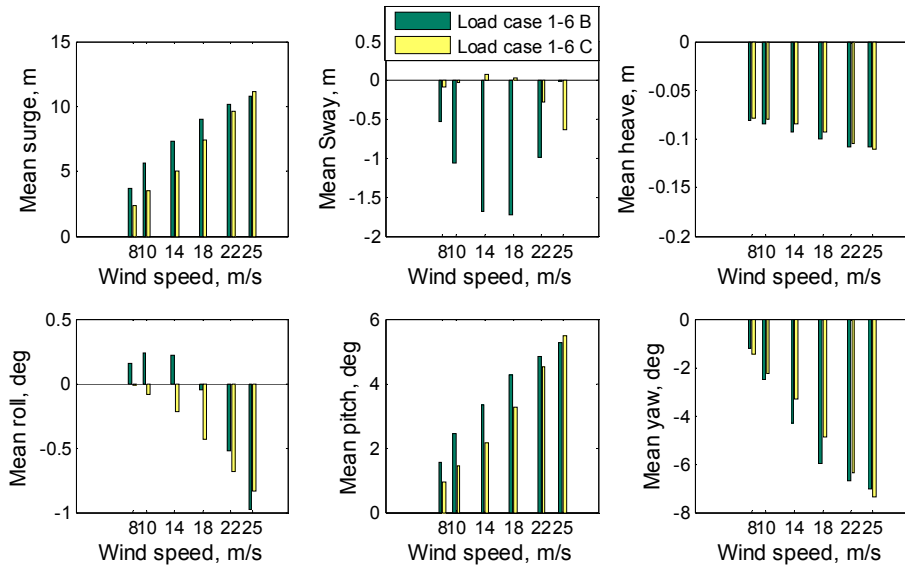


Fig.10: Mean values of the platform motions under the fault-free case and fault case C for all wind speeds

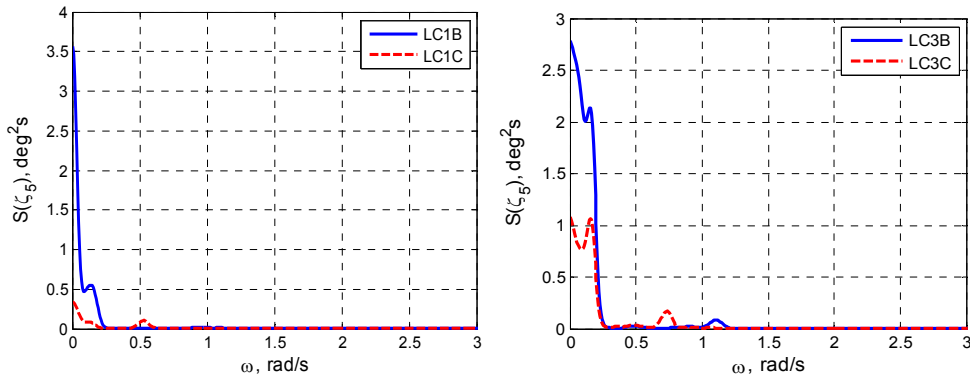


Fig. 11: Power spectra for pitch motion of the platform for load cases 1 and 3 with fault configurations B and C

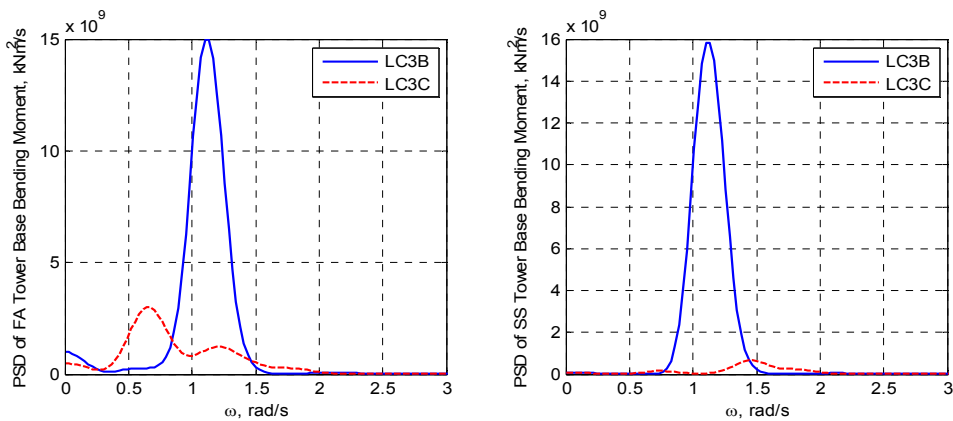


Fig. 12: Power spectra for FA and SS tower base moment for load case 3 with fault configurations B and C

4.3. Investigation of the Shutdown Process by Using Hydrodynamic Brake II and Mechanical Brake

Hydrodynamic brake II features a larger plate width than hydrodynamic brake I and can exert greater torque on the rotating shaft. After hydrodynamic brake II was applied in the FVAWT, the rotational speed in all load cases at different wind speeds could be rapidly reduced to a very low value. Then, the mechanical brake could be applied on the brake disk to stop the rotation of the wind turbine 200 s after the fault occurred. The value of the mechanical brake torque was assumed to be twice the value used in the NREL reference wind turbine and was set to 5454.5 kNm for a low speed shaft. Until the wind turbine was completely shut down, the process remained transient, and the platform gradually moves toward its final equilibrium position with some delay after the rotational speed, as shown in Fig. 13. The figure shows that the combination of the hydrodynamic brake and mechanical brake can effectively complete an emergency shutdown. It should be noted that the global motion, bending moment and tension of the mooring lines after the shutdown of the wind turbine can also vary under several factors, such as wind speed, wave condition and control strategy, because the aerodynamic loads depend on the azimuthal angle of the blades in the equilibrium position.

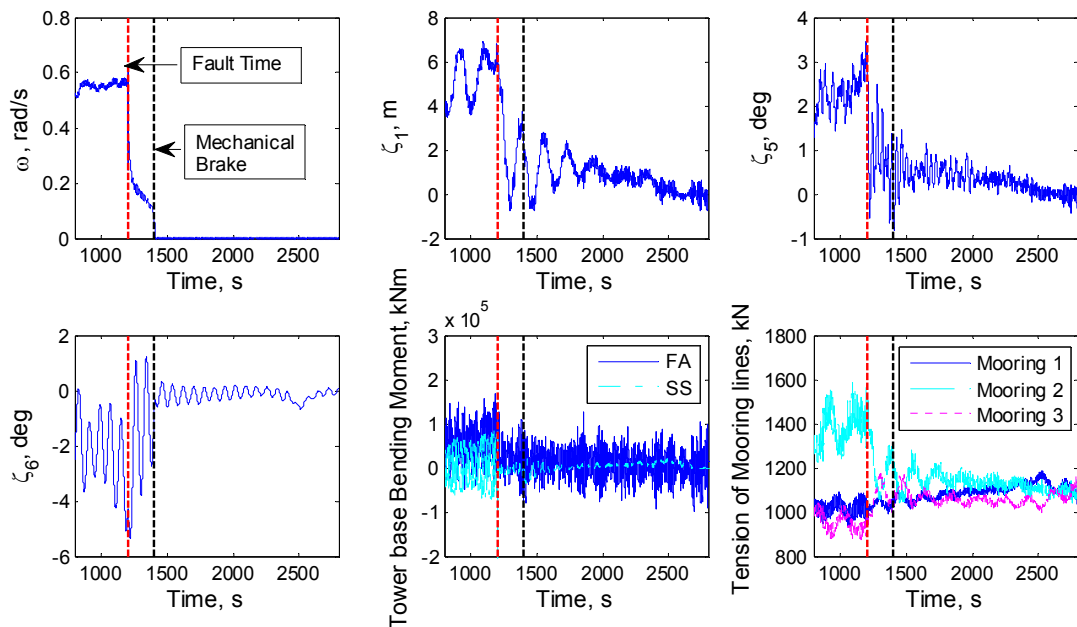


Fig. 13: Time history of the rotational speed, surge, pitch, yaw, tower base bending moments and mooring line tension for load case 2D

5. Conclusions

In the present work, a coupled non-linear time domain code was used to carry out numerical simulations for a floating vertical axis wind turbine with a hydrodynamic brake. To integrate the hydrodynamic brake into the original FVAWT, the hydrodynamic brake was modeled by a slender line, whose the hydrodynamic coefficient includes the added mass and drag coefficient. Furthermore, the torque of the hydrodynamic brake from the water was also calculated by a CFD model for different rotational speeds. Based on the integrated model, a series of load cases were selected to investigate the effect of the hydrodynamic brake and shutdown process for the wind turbine under normal operating conditions. The dynamic analysis focused on the comparison of global motions, tower base bending moments and the tensions of mooring lines for different load cases with different fault configurations.

The effect of the hydrodynamic brake on the FVAWT was evaluated by comparing the results obtained for the FVAWT with hydrodynamic brake I with the results obtained for the original FVAWT under normal operating conditions.

The addition of the hydrodynamic brake does not affect the surge motion as long as the wind speed is not too high. Otherwise, the surge motion induced by the wind can be greatly reduced by the drag force on the hydrodynamic brake. It was observed that the sway motion could be affected by the drag force on the brake when the yaw degree of freedom was presented. The effect on the roll and pitch motions also depends on the wind speed and is slightly complex because both the natural frequency and 2P frequency both affect the responses. From a structural point of view, the brake has a greater positive effect on the mooring lines, but it could enlarge the 2P effect on the tower base bending moment. This finding indicates that a better hydrodynamic brake design is critical to reducing the 2P effect on the tower base bending moment by avoiding the stiffening of the platform.

By investigating the shutdown process following the activation of the hydrodynamic brake to decelerate the wind turbine, a series of promising results revealed the merits of the hydrodynamic brake for the emergency shutdown. As long as the rotational speed can be reduced to relatively lower values, the global motion and structural responses can both be reduced. Although the same wave and wind conditions were applied to compare the results of different fault configurations and one realization of each load case could lead to certain uncertainties in the mean values and standard deviations of the global motions and structural responses, the results obtained from the comparison of the different fault configurations for each load case are still sufficient for evaluating the effect of the hydrodynamic brake on the FAVWT during the shutdown process.

By combing a mechanical brake with a larger hydrodynamic brake, the shutdown process could be successfully completed. The application of a hydrodynamic brake is expected to be efficient for rotor shutdown and for reducing the platform motion and structural loads.

Acknowledgments

The authors would like to acknowledge the financial support from the Research Council of Norway through NOWITECH and the Centre for Ships and Ocean Structures at the Department of Marine Technology, Norwegian University of Science and Technology, Trondheim, Norway.

References

- [1] Paulsen, U.S., et al. Deepwind - An innovative wind turbine concept for offshore. in *European Wind Energy Association (EWEA) Annual Event*. 2011. Brussels.
- [2] Vita, L., Paulsen, U.S., and Pedersen, T.F. A novel floating offshore wind turbine concept: new developments. in *European Wind Energy Conference and Exhibition*. 2010. Poland: EWEA.
- [3] Vita, L., et al. A novel floating offshore wind turbine concept. in *European Wind Energy Conference and Exhibition*. 16-19 March, 2009. Marseille, France: EWEC.
- [4] Cahay, M., et al. Use of a Vertical Wind Turbine in an Offshore Floating Wind Farm. in *Offshore Technology Conference* 2-5 May 2011. Houston, Texas, USA: Offshore Technology Conference.
- [5] 10MW Aerogenerator X © Wind Power Limited & Grimshaw at <http://vimeo.com/13654447>.
- [6] Paulsen, U.S., et al., 1st DeepWind 5 MW Baseline design. *Energy Procedia*, 2012. **24**: p. 27-35.
- [7] Robertson, A., et al., Definition of the Semisubmersible Floating System for Phase II of OC4, 2012.
- [8] Wang, K., Moan, T., and Hansen, M.O.L. A method for modeling of floating vertical axis wind turbine. in *Proceedings of the 32th International Conference on Ocean, Offshore and Arctic Engineering*. 2013. Nantes, France: paper no: OMAE2013-10289.
- [9] Coulling, A.J., et al., Validation of a FAST semi-submersible floating wind turbine numerical model with DeepCwind test data. *Journal of Renewable and Sustainable Energy*, 2013. **5**: p. 023116.
- [10] Vita, L., Offshore Floating Vertical Axis Wind Turbines with Rotating Platform, in *Risø-PhD-80(EN)2011*, National Laboratory for Sustainable Energy, DTU.
- [11] Ormberg, H., Passano, E., and Luxey, N. Global analysis of a floating wind turbine using an aero-hydroelastic model. Part 1: Code development and case study. in *Offshore Mechanics and Arctic Engineering Conference*. 2011. Rotterdam, The Netherlands.
- [12] Luxey, N., Ormberg, H., and Passano, E., Global analysis of a floating wind turbine using an aero-hydro-elastic numerical model. Part 2: Benchmark study, in *Offshore Mechanics and Arctic Engineering Conference* 2011: Rotterdam, The Netherlands.
- [13] Wang, K., Hansen, M.O.L., and Moan, T., Model improvements for evaluating the effect of tower tilting on the aerodynamics of a vertical axis wind turbine. *Wind Energy*, 2013.
- [14] Svendsen, H.G., Merz, K.O., and Endegnanew, A.G. Control of floating vertical axis wind turbine. in *European Wind Energy Conference and Exhibition* 2012. Copenhagen, Denmark: EWEA.
- [15] Det Norske Veritas, ENVIRONMENTAL CONDITIONS AND ENVIRONMENTAL LOADS, Tech. Rep., DNV-RP-C205 (2007).
- [16] International Electrotechnical Commission (2009). *IEC61400-3 Wind turbines - Part 3: Design requirement for offshore wind turbines*.

- [17] Johannessen, K., Meling, T.S., and Haver, S., Joint distribution for wind and waves in the northern north sea. *International Journal of Offshore and Polar Engineering*, 2002. **12**(1).
- [18] MARINTEK, SIMO User's Manual, 2011.
- [19] Jiang, Z., Karimirad, M., and Moan, T., Dynamic response analysis of wind turbines under blade pitch system fault, grid loss, and shutdown events. *Wind Energy*, 2013.
- [20] Vakili, M. and Esfahany, M.N., CFD analysis of turbulence in a baffled stirred tank, a three-compartment model. *Chemical Engineering Science*, 2009. **64**(2): p. 351-362.
- [21] Deglon, D. and Meyer, C., CFD modelling of stirred tanks: Numerical considerations. *Minerals Engineering*, 2006. **19**(10): p. 1059-1068.
- [22] Ankamma Rao, D. and Sivashanmugam, P., Experimental and CFD simulation studies on power consumption in mixing using energy saving turbine agitator. *Journal of Industrial and Engineering Chemistry*, 2010. **16**(1): p. 157-161.
- [23] Aubin, J., Fletcher, D.F., and Xuereb, C., Modeling turbulent flow in stirred tanks with CFD: the influence of the modeling approach, turbulence model and numerical scheme. *Experimental Thermal and Fluid Science*, 2004. **28**(5): p. 431-445.
- [24] Sato, Y., Nakamura, H., and Watano, S., Numerical analysis of agitation torque and particle motion in a high shear mixer. *Powder Technology*, 2008. **186**(2): p. 130-136.
- [25] Knight, P., et al., Prediction of impeller torque in high shear powder mixers. *Chemical Engineering Science*, 2001. **56**(15): p. 4457-4471.